Resistance to Blood Flow in Microvessels In Vivo

A.R. Pries, T.W. Secomb, T. Geßner, M.B. Sperandio, J.F. Gross, P. Gaehtgens

Abstract Resistance to blood flow through peripheral vascular beds strongly influences cardiovascular function and transport to tissue. For a given vascular architecture, flow resistance is determined by the rheological behavior of blood flowing through microvessels. A new approach for calculating the contribution of blood rheology to microvascular flow resistance is presented. Morphology (diameter and length), flow velocity, hematocrit, and topological position were determined for all vessel segments (up to 913) of terminal microcirculatory networks in the rat mesentery by intravital microscopy. Flow velocity and hematocrit were also predicted from mathematical flow simulations, in which the assumed dependence of flow resistance on diameter, hematocrit, and shear rate was optimized to minimize the deviation between measured and predicted values. For microvessels with diameters below ≈40 μm, the resulting flow resistances are markedly higher and show a stronger dependence on hematocrit than previously estimated from measurements of blood flow in narrow glass tubes. For example, flow resistance in 10-μm microvessels at normal hematocrit is found to exceed that of a corresponding glass tube by a factor of ≈4. In separate experiments, flow resistance of microvascular networks was estimated from direct measurements of total pressure drop and volume flow, at systemic hematocrits intentionally varied from 0.08 to 0.68. The results agree closely with predictions based on the above-optimized resistance but not with predictions based on glass-tube data. The unexpectedly high flow resistance in small microvessels may be related to interactions between blood components and the inner vessel surface that do not occur in smooth-walled tubes. (***Circ Res.* 1994;75: 904-915.**)

Key Words • blood viscosity • peripheral resistance • microvascular networks • pressure drop • hematocrit

Early in the 19th century direct measurements of arterial and venous blood pressure by Jean Léonard Marie Poiseuille[1,2] revealed that the pressure drop in the circulation occurs mainly in the peripheral vascular bed (the microcirculation), which consists of large numbers of tiny vessels. The microcirculation is therefore the site of most of the resistance to flow, which depends on the architecture of the microvascular network and on the rheological behavior of blood flowing through it. Information about bulk rheological properties of blood has been obtained using rotational viscometers. The findings of such studies, including the nonlinear increase of viscosity with increasing hematocrit and with decreasing shear rate,[3-5] have strongly influenced the interpretation of physiological and pathophysiological behavior of the peripheral circulation.

However, knowledge of the bulk material properties of blood does not provide a sufficient basis for understanding blood flow through narrow cylindrical tubes. In tubes with diameters >1 mm, the measured apparent viscosities correspond to bulk values from rotational viscometry, but a marked reduction of viscosity is observed with decreasing tube diameter, the so-called Fahraeus-Lindqvist effect.[6,7] In the diameter range from ≈5 to 15 μm, apparent blood viscosity is only slightly higher than that of the suspending plasma and does not exhibit a strong dependence on hematocrit.[8-13]

If extrapolated to the microcirculation, these in vitro results imply that apparent viscosity is very low in those vessels that contribute most to overall flow resistance. The question whether in vitro measurements of apparent viscosity also provide adequate estimates of flow resistance in the microcirculation is therefore of great significance, both for physiological concepts of peripheral circulation and for assessment of pathophysiological processes and therapeutic interventions. Although narrow blood-perfused glass tubes approximate in vivo conditions more closely than do rotational viscometers, they nevertheless differ in several respects from the relatively short, irregularly shaped, endothelium-lined vessels in microvascular networks.

Direct measurements of flow resistance in single unbranched microvessels are technically difficult, and the derived apparent viscosities suffer from considerable measurement errors. However, available data[14-16] for diameters <40 μm suggest that the strong reduction of viscosity with decreasing diameter predicted by the Fahraeus-Lindqvist effect seen in vitro is not present to the same extent in living microvessels. Such data suggest that experimental measurements in glass tubes do not provide a reliable basis for predicting the effective viscosity of blood in vivo. (Effective viscosity of blood flowing through a living vessel is defined here as the viscosity calculated from Poiseuille's equation for the observed pressure drop along the vessel, the average vessel diameter, and the vessel length. Relative effective viscosity is given by dividing this value by the viscosity of plasma. This is equivalent to the flow resistance observed in the blood-perfused vessel divided by that of a cylindrical tube of the same length and diameter perfused with plasma.)

In the present study, a new approach is used to determine the effective viscosity and its dependence on

Received March 7, 1994; accepted August 3, 1994.

From the Department of Physiology, Freie Universität Berlin (Germany) (A.R.P., T.G., M.B.S., P.G.), and the Department of Physiology, University of Arizona, Tucson (T.W.S., J.F.G.).

Correspondence to Axel R. Pries, MD, Freie Universität Berlin, Department of Physiology, Arnimallee 22, D-14195 Berlin, Germany.

vessel diameter and hematocrit in microvessels of a living tissue. This approach was made possible by the development of experimental methods for the measurement of hematocrit and flow velocity in all vessel segments of large microvascular networks, in conjunction with theoretical simulations of blood flow through these networks based on the experimentally determined architecture. The overall deviations between measured and predicted hematocrits or velocities were used as criteria to optimize the assumptions made in the simulation concerning the effective viscosity of blood. By minimizing the respective deviations, an optimal approximation to the blood rheology in living microvessels was achieved. Although this method represents an indirect approach to the evaluation of in vivo effective viscosity, it has the advantage that the assessment is based on a summation of deviations from a large number of segments (up to 913) per network. This renders the method relatively insensitive to random measurement errors of relevant quantities in individual vessel segments and allows a parametric description of effective viscosity as a function of vessel diameter and hematocrit, which is called the "in vivo viscosity law."

To test the validity of the respective results, an additional series of experiments was performed in which the pressure drop across microvascular networks was directly measured by micropipette techniques. In addition, the dependence of overall network flow resistance on systemic hematocrit was determined. These data were compared with predictions of model simulations based on the in vivo viscosity law.

Materials and Methods

Experimental Network Data

Details of the animal preparation and experimental setup,[17] the intravital microscope,[18] the data gathering and scanning procedure,[17] and the optical method for hematocrit determination[19] have been described previously. Male Wistar rats (n=6; body weight, 300 to 450 g) were anesthetized with ketamine (100 mg/kg IM) after premedication (0.1 mg/kg IM atropine and 20 mg/kg IM pentobarbital sodium). During the experiment, an intravenous infusion (24 mL/kg per hour) of physiological saline containing 0.3 mg/mL pentobarbital sodium was administered to maintain fluid balance and anesthetic level. Arterial blood pressure (range, 105 to 140 mm Hg) and heart rate were monitored continuously.

Fat-free portions of the mesenteric membrane (area ranging from 25 to 80 mm^2) were exposed for intravital videomicroscopy, scanned, and recorded on videotape and on black and white film. To abolish the potential development of tone during the experiments, papaverine (10^{-4} mol/L, Serva) was continuously applied via the solution superfusing the investigated tissue. In all six networks investigated, a scan was performed by using monochromatic continuous illumination at a wavelength of 448 nm to allow densitometric hematocrit measurements. A Leitz SW 25/0.6 saltwater immersion objective yielded a final magnification at the photodetector level of $\approx\times 28$. The complete scan took $\approx$30 minutes and consisted of $\approx$300 individual fields of view (300×400 μm).

In three of the six networks investigated, the flow velocity in each vessel segment was determined. An additional second scan was performed by use of a strobed asynchronous illumination to allow off-line velocity measurement with a digitized image analysis system.[20,21] The analysis of velocity is based on the principle of spatial correlation[22]: The light intensity pattern along a line in the center line of the image of a microvessel is determined at two closely spaced time instances. If the vessel contains moving blood cells absorbing and scattering light, the corresponding intensity patterns are shifted in position between the two successive recordings. The center-line flow velocity (v_{cl}) is obtained by dividing the length of this spatial shift by the time delay between the two recordings.

Because of the periodicity of the intensity signals created by flowing blood cells, a reliable determination of the spatial shift can, under most experimental conditions, only be obtained for shifts below $\approx$20 μm. Therefore, the upper limit of the velocity measurement depends on the time delay between the recordings, which is 20 or 16.67 milliseconds for a 50- or 60-Hz operation, respectively, corresponding to maximal velocities of $\approx$1 or 1.2 mm/s. This would be too low to allow an analysis of flow velocities in many of the microvessels present in the rat mesentery. Therefore, we used an asynchronous flash illumination system (11360-1, Chadwick-Helmuth) illuminating one half frame by a flash immediately preceding the frame transfer of the recording CCD camera (model MX, AIS). The next flash is then triggered after a short delay (eg, 1 millisecond) and illuminates the next half frame. A much longer delay (eg, 39 milliseconds for a 50-Hz operation) follows until the next double flash pulse is started. Whereas the video image recorded with this illumination system can be stored and replayed at the normal framing rate on standard video equipment, every other pair of two successive half frames represents images created at time delays of only 1 millisecond in real time. With the minimum delay of 0.5 millisecond used in the present study, the maximum measurable flow velocity ranged $\approx$40 mm/s.

Each field of view was recorded during asynchronous flash illumination for $\approx$10 seconds. For the off-line analysis of velocity, a measuring line was interactively defined along the axis of the respective vessel segment during replay of the videotape. A sequence of $\approx$100 pairs of line intensity patterns was extracted from the recordings, corresponding to a recording time of 4 seconds, by using a digital image analysis system.[20] The spatial shift between each of the line pairs was then automatically determined by means of a cross-correlation procedure and converted into v_{cl}. Periodic changes of flow velocity coupled to heart rate and breathing were eliminated by averaging velocities over the complete sequence recorded.

Averaged v_{cl} values determined by spatial correlation were then converted into mean blood velocity (v_b). For single-file flow conditions, v_{cl} can be assumed to be identical to mean cell velocity (v_c). The relation between v_c and v_b, in turn, is identical to the relation between discharge hematocrit (H_D) and tube hematocrit (H_T), given by the Fahraeus effect. To calculate v_b/v_c, a parametric description of the Fahraeus effect as a function of vessel diameter (D, in micrometers) and hematocrit derived from a compilation of literature data on red blood cells perfused through glass tubes of different diameters[23] was used:

$$(1)\quad \frac{v_b}{v_c} = H_D + (1-H_D)\cdot(1+1.7e^{-0.415D}-0.6e^{-0.011D})$$

In larger microvessels, several red blood cells may travel on one vessel cross section at different velocities. In this situation, v_{cl} represents some average of the velocities in a vertical section through the vessel. According to Pittman and Ellsworth,[24] the relation between v_b and v_{cl} depends on the velocity profile in the vessel investigated, which is described by a bluntness factor, the size of flowing erythrocytes, and the width of the area from which light is sampled for velocity measurement. In the present study, we assumed a bluntness factor of 0.8, representing a rough mean of the experimental data cited by Pittman and Ellsworth, an erythrocyte diameter of 5 μm, and a width of the light-sampling area of 1 μm.

For vessels with diameters <5 μm, the relation between v_b and v_{cl} was exclusively derived from the Fahraeus effect equation, whereas for vessels >40 μm, the Pittman and Ellsworth[24] approximation was used. In the intermediate

range, a smooth linear transition between the values given by both approaches was used. For an H_D of ≈0.45, the resulting values for v_b/v_{cl} range between 0.73 and 0.75 down to diameters of ≈7 μm and increase steeply toward unity below that level. For very low hematocrits, however, much lower values for v_b/v_{cl} are obtained in the diameter range of ≈10 μm because of the hematocrit dependence of the Fahraeus effect.

The photographs exposed during the scanning procedure were used to assemble photomontages of the complete microvascular networks, which were then used to determine network topological structure (connection matrix) and the length of all vessel segments between branch points. The diameter of vessel segments was determined from the video recordings obtained with the strobed flash illumination, where available (n=3 networks), and from the photonegatives for the remaining networks (n=3). The number of vessel segments per network varied between 383 and 913.

Network Flow Simulation

Details of the flow simulation have been described earlier.[23] Based on the experimentally determined network topology (connection matrix) and architecture (diameter and length of each vessel segment) plus the hemodynamic conditions in vessel segments entering or leaving the network (boundary conditions), an iterative algorithm was used to calculate pressures at each branch point within the network as well as flow rates and hematocrits in each vessel segment. The boundary conditions comprise the volume flow rates and hematocrits in all vessel segments feeding the network and the volume flow rates for those segments leaving the network, with the exception of the main venular draining segment. This segment was arbitrarily assigned a pressure of 0 mm Hg to provide a fixed pressure reference point in the network.

For those networks in which flow velocities were not measured, v_b (in millimeters per second) for the main arteriolar input segments was assigned according to segment diameter D using the following equation[23]:

$$v_b = 0.4 \cdot D - 1.9 \quad (2)$$

This equation yields flow velocities close to those measured experimentally for similar sized vessels. For other inflow and outflow segments, volume flow rates were derived from the value assigned to the main feed arteriole according to the relative number of capillary segments fed or drained.

In addition to the input information on network architecture and boundary conditions, the model simulations rely on parametric descriptions of rheological phenomena in the microcirculation. These are the phase-separation effect (nonproportional partition of red blood cell and plasma flows) at diverging bifurcations and the effective viscosity of blood flowing through microvessels. A parametric description of phase separation (phase-separation law), which is based on experimental data obtained previously in arteriolar bifurcations of the rat mesentery[25] (Equations 4 through 6 in Reference 23), was used. This law describes the distribution of blood and red blood cell flow at individual bifurcations.

The in vitro viscosity law used in the present study is based on a previous compilation of literature data on relative blood viscosity in tube flow in vitro.[13] This is described by the following equation:

$$\eta_{vitro} = 1 + (\eta_{0.45} - 1) \cdot \frac{(1-H_D)^C - 1}{(1-0.45)^C - 1} \quad (3)$$

where η_{vitro} is in vitro viscosity and $\eta_{0.45}$, the relative viscosity for a fixed H_D of 0.45, is given by

$$\eta_{0.45} = 220 \cdot e^{-1.3D} + 3.2 - 2.44 \cdot e^{-0.06D^{0.645}} \quad (4)$$

Equation 4 is a description of the diameter dependence of viscosity in tube flow, the so-called Fahraeus-Lindqvist effect. C describes the shape of the viscosity dependence on hematocrit and is given by the following equation:

$$C = (0.8 + e^{-0.075D}) \cdot \left(-1 + \frac{1}{1 + 10^{-11} \cdot D^{12}}\right) + \frac{1}{1 + 10^{-11} \cdot D^{12}} \quad (5)$$

This relation gives a linear dependence between viscosity and hematocrit for diameters <7 μm and a strong nonlinear increase of viscosity with hematocrit for diameters >8 μm.

Experimental Determination of Network Flow Resistance

To obtain experimental data that can be used to validate results of the network flow simulations, pressure drop and volume flow rates across microvascular networks in the rat mesentery were measured at different levels of systemic hematocrit (H_S) in a separate series of experiments (n=10). The networks chosen were similar to those used to obtain network data, and the details of the animal preparation and intravital microscopy correspond to those described above. One field of view was observed, including the main feeding arteriole and, in most experiments, the paired draining venule. To block alterations of vascular tone during the experiments, papaverine (10^{-4} mol/L) was added to the superfusion solution throughout the experiments. A micropipette with a tip diameter of ≈1 μm connected to a micropressure measuring system (model 5, IPM) was impaled into the arterioles or the venules to measure intravascular pressure according to the servo-nulling technique.

A typical experiment started with the measurement of venular pressure. Next, the micropipette was introduced into the main feeding arteriole, and pressure was measured, while video recordings were taken by using asynchronous flash illumination to allow an off-line determination of arteriolar v_{cl} and thus calculations of volume flow rate. In some experiments, H_S was increased to up to 0.65 by slow infusion of concentrated red blood cells (≈5 mL) obtained from another rat. Systemic hematocrit was then lowered by successive hemodilution. This was achieved by replacing aliquots of blood (1 to 2 mL) drawn from the carotid catheter with homologous plasma infused intravenously. At low levels of H_S, hydroxyethyl starch solution (100 g/L; molecular weight, 200 000/0.5 in physiological saline; Fresenius) was given in addition to plasma in quantities of <2 mL per dilution step to increase the dilutive effect and to limit the fall in arterial pressure.

After each hemodilution step, the measurements of arterial pressure and flow velocity in the arteriole observed were repeated. The experiment was completed by a measurement of venular pressure at the lowest hematocrit level reached. Since venular pressure showed little or no change, venular pressure levels for the intermediate hematocrit steps were interpolated from the values taken at the beginning and the end of the experimental procedure. Arteriolar flow velocities were converted into volume flow rates by using the diameter measured off-line from the video recordings. Dividing the arteriovenous pressure drop values across the microvascular networks by the arteriolar volume flow rate yielded overall network flow resistance for every level of H_S.

To allow a comparison of the data obtained from networks of different size and geometrical hindrance, the resistance values of each data set were normalized with respect to the resistance (R_0) for pure plasma perfusion (H_S=0). The lowest levels of H_S reached in the experimental determinations of network resistance were ≈0.15. To extrapolate the flow resistance to zero hematocrit, each set of experimental data was fitted by an equation similar to that used to describe the dependence of relative blood viscosity as a function of hematocrit (Equation 3 in Reference 13):

$$R = A + B \cdot (1 - H_S)^C - 1) \quad (6)$$

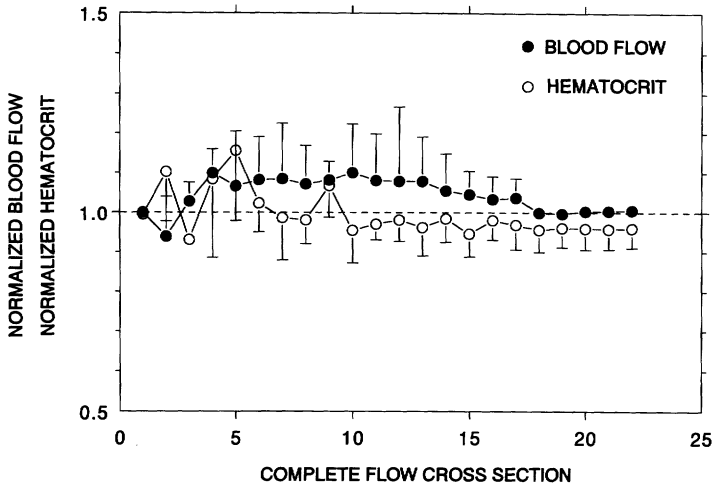

FIG 1. Graph showing mass conservation in the data sets of volume flow and hematocrit. For three networks in which flow velocity and discharge hematocrit were measured throughout, blood volume flow and flow-weighted discharge hematocrit (mean±SD) are given for successive arteriolar complete-flow cross sections. Data were normalized with respect to the flow, and hematocrit values were measured in the main feeding arterioles or flow cross section 1. The subsequent flow cross sections consist of vessel segments of the corresponding generation level plus all lower generation capillaries. Red blood cell and plasma flows are corrected for contributions from segments leaving the boundaries of the tissue region scanned. The mean deviations from perfect mass conservation are <5% for both parameters, and no systematic trend toward distal flow cross sections is seen.

where R is the flow resistance. Parameter A of the fit corresponds to the resistance for $H_S=0$; B and C give the steepness and shape of the relation between H_S and R. In two data sets, negative values of A were obtained, and the lowest experimental value of R was substituted for R_0 instead of A.

Results

Network Experiments

In the present study, measured segment flow velocities and hematocrits are used to test the adequacy of viscosity laws applied in the simulation. Therefore, it is important to test whether these quantities suffer from systematic measurement errors. Such errors could result, for example, from a systematic bias in the measurement of vessel diameter or in the relation between true and estimated mean v_b. Errors leading to proportional changes of calculated blood (red blood cell) volume flow in all segments would be of minor importance for the conclusions drawn. If, in contrast, the bias were to vary systematically with vessel diameter, hematocrit, or flow velocity, this would have a direct impact on the in vivo viscosity law derived.

The experimental data for the three networks in which velocity data had been obtained experimentally were tested for such inconsistencies. In each, the blood volume flow and the flow-weighted mean H_D were calculated for a series of consecutive complete flow cross sections, through which all the blood entering the network must pass. Each flow cross section consists of the arterioles of a given generation plus all capillaries up to that generation.[17] The generation of a vessel segment is the number of bifurcations between that vessel and the input segment of the network plus one. The flow and hematocrit values for each flow cross section were corrected for the volume flow and hematocrit in arteriolar segments, leaving the network at lower generation levels.

Mass conservation implies that both flow and flow-weighted mean hematocrit are unchanged in each of these complete flow cross sections. As shown in Fig 1, the deviation of average experimental results from that ideal behavior is small and shows no consistent trend from proximal to distal flow cross sections. The volume flow of blood and red blood cells that enter the network by the few fast-flowing large arterioles is obviously completely recovered at the level of the many small slow-flowing capillaries, although the latter exhibit a large range of individual segment hematocrits. Therefore, the existence of systematic errors in diameter and hematocrit measurement related to vessel diameter, hematocrit, or flow velocity is unlikely to be present to a substantial degree.

In addition, conservation of volume flow rate was checked for all arteriolar branch points in the three networks in which flow velocity was measured (n=137±11 per network). The summed flow in the daughter branches exceeded that in the mother vessel, on average by 0.014 nL/min (SD between networks, 0.046 nL/min) with an average SD within the individual networks of 10.5 nL/min. When the average volume flow at arteriolar branch points (25.7±11.2 nL/min for 412 bifurcations in three networks) was taken into account, the average relative deviation is 0.0003 with an SD within networks of 0.43. This indicates that no systematic violation of mass conservation is obvious from the measured flow velocities and vessel diameters, despite the fairly large errors at individual bifurcations, and supports the idea that summations of data from multiple segments are relatively insensitive to random measurement errors in individual segments.

Comparison of Experimental Results and Model Predictions

Segment-by-segment comparisons between measured and predicted values of velocity and hematocrit measured in a network with 546 segments are shown in Fig 2. The predicted values were obtained by the flow simulation model using the in vitro viscosity law. Flow velocity and especially hematocrit show large deviations between predicted and measured results. The fairly large deviations between measured and predicted flow velocity and hematocrit can be attributed to at least three independent error sources: the measurement error, the model input error, and the rheological law error.

To permit evaluation of alternative models, numerical measures of these deviations were obtained. Velocity varies over a wide range, so root mean square (rms) relative velocity deviation was used. For each segment, relative deviation was computed as the difference between measured and predicted velocities divided by the mean of these two values. The mean was used here,

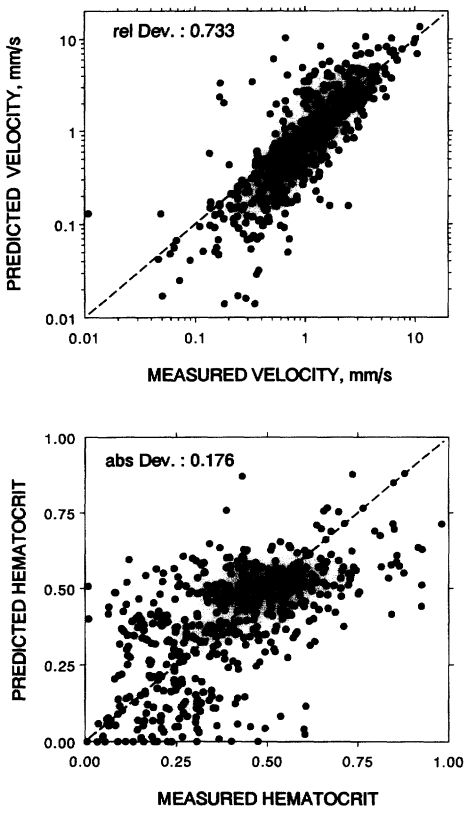

FIG 2. Scatterplots comparing flow velocity (top) and hematocrit (bottom) as measured directly in vessel segments (n=546) of a microvascular network in the rat mesentery with the corresponding predictions of the flow simulation model based on the in vitro viscosity law (black dots). In addition, lines of identity are shown. The mean relative deviation (rel Dev.) of velocity was calculated as the root mean square (rms) of the difference between measured and predicted velocities divided by their average over all vessel segments. The absolute hematocrit deviation (abs Dev.) is the rms difference between measured and predicted discharge hematocrit values.

since both velocities are subject to errors. In contrast to velocity, hematocrit lies within a defined range (0 to 1), so the absolute hematocrit deviation was used. The choice of these measurements is supported by Fig 2, which shows that deviations in velocity and hematocrit are roughly constant in magnitude over the range of observed values when hematocrit is plotted on a linear scale and velocity is plotted on a logarithmic scale. For the three networks in which velocities were measured, relative rms averaged 0.723±0.058 (mean±SEM, n=3). Hematocrit deviations (rms) averaged 0.173±0.009 for six networks.

Measurement Error

To assess the measurement errors of the optical methods used to determine flow velocity and hematocrit, double measurements of both quantities were performed in a large number (n=190) of segments in one of the networks analyzed. From the obtained values, conservative estimates of relative rms velocity error of 0.25 and absolute rms hematocrit error of 0.11 were derived and used in the following analysis.

Model Input Error

Stochastic errors in the input information will indirectly result in deviations between measured and predicted values, in addition to those created by the direct measurement errors of velocity and hematocrit described above. One component of the model input error is caused by incorrect values of segment length and diameter in the morphological data used in the network flow simulation. The second part of this error relates to the phase-separation law used to define the phase-separation parameters at individual bifurcations. The original data used to derive the parametric description of phase separation[25] show a fairly large scatter around the reported average values, which is probably due to the fact that relevant parameters including the microgeometry of the bifurcation as well as the radial velocity and hematocrit profile in the feeding vessel were not represented in the bifurcation law.

The impact of model input errors on the deviation between measured and predicted parameters was assessed by comparing the results of simulation runs based on the standard input set for a given network with those of runs in which the segment diameters and lengths as well as the individual phase-separation parameters were modified according to the characteristic uncertainty ranges. These modifications consisted of randomizing the respective parameters relative to the standard values given by the input database (segment diameter and length) and the parametric description of phase separation according to their empirically determined error ranges. A relative rms error of ±0.07 (7%) for segment lengths and an absolute rms error of ±1.2 μm for segment diameters were used according to double measurements (n=240) in one of the networks investigated. For the three phase-separation parameters, A, B, and X_o, the standard deviations of data obtained at individual bifurcations from the predictions of the phase-separation law, as calculated from the original data given by Pries et al,[25] were used (A, ±0.45; B, ±0.3; and X_o, ±0.05).

For each of the 100 randomized runs performed per network, the mean deviation between flow velocities and hematocrits in the individual segments and those values obtained with standard parameters was determined and averaged for each network. A relative rms error of 0.518±0.037 (mean±SEM, n=3) for velocity and an absolute rms error of 0.102±0.008 (hematocrit units, n=6) for hematocrit were obtained. These values were used as an estimate for the impact of model-input errors on the overall deviation between measured and predicted values of flow velocity and hematocrit.

Rheological Law Error

The remaining possible source for the deviation between measured and predicted values is a systematic error in the rheological laws, particularly the assumed variation of flow resistance with microvascular diameter and hematocrit (the viscosity law). The part of the overall deviation that cannot be accounted for by the stochastic measurement error or the model input error, as described above, must be attributed to systematic rheological law error.

In Fig 3, the contributions of the three components of overall deviation between measured and predicted flow velocities and hematocrits are shown. Values have been normalized with respect to the deviation found with the in vitro viscosity law (n=3 for velocity, n=6 for hematocrit). In addition, values are given here as mean-square

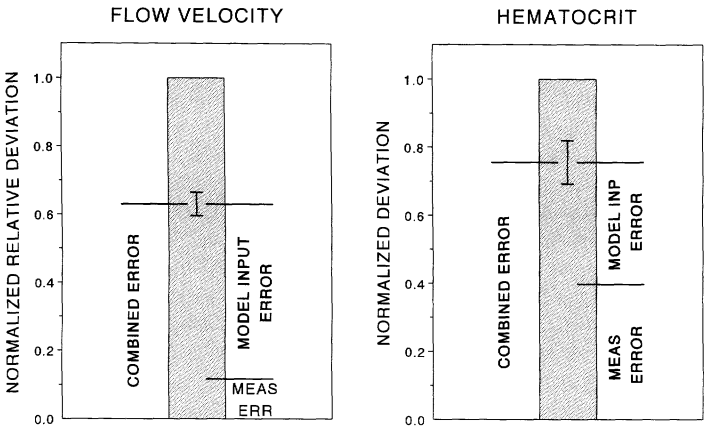

FIG 3. Bar graphs showing components of the deviation between measured and predicted flow velocity (left, n=3 networks) and hematocrit (right, n=6) given as mean-square deviations and normalized with respect to the overall deviation of the individual networks. The random measurement error (meas err) in the respective variable (velocity or hematocrit) and the deviation caused by stochastic errors in the input databases used in the model simulations (model input [inp] error) yield the combined stochastic error, which is indicated by horizontal lines (±SEM). The remaining deviation is attributed to the systematic incorrectness of the rheological laws used for the model simulations.

deviations (variance) rather than as rms deviations (SD) to allow the addition of measurement error and model input error to yield a combined stochastic error (combined error). The remaining part of the deviation, referred to as systematic deviation, must be primarily due to systematically incorrect assumptions in the viscosity law used in the simulations. The size of this error provides an index that can be used to test the correctness of alternative forms of the viscosity law.

Evaluation of the In Vivo Viscosity Law

Effects of changes in the viscosity law on the systematic deviation between measured and predicted flow velocity and hematocrit were analyzed. For all tested viscosity laws, the respective systematic deviations were compared with those obtained for the standard in vitro viscosity relation as shown in Fig 4 (in vitro law).

Also shown are results obtained with a viscosity law incorporating a shear-dependent component of viscosity, according to data published by Reinke et al[26] based on perfusion experiments in vertical glass tubes, which predict a weak dependence of viscosity on shear rate. The shear-rate dependence was introduced into the model simulation by multiplying the viscosity as obtained from the in vitro viscosity law (Equation 3) with a velocity-dependent term:

$$\eta_{shear} = \eta_{vitro} \cdot (P \cdot \bar{U}^{Q} + 1) \quad (7)$$

where η_{shear} is the shear-rate–dependent relative viscosity, $\bar{U}$ is the shear rate (v_b/D), and P and Q are parameters of the exponential fit to the original data given by Reinke et al (P, 0.25; Q, −0.85). Based on this relation between shear rate and viscosity, the deviations of velocity and hematocrit are very close to those found with the standard in vitro law. Alternatively, we applied a shear-dependent viscosity component according to that used by Warnke and Skalak[27] in their hydrodynamic flow model, which is based on in vivo experimental data by Lipowsky and coworkers.[14,15] This strongly shear-rate–dependent viscosity law yielded substantial increases in the deviation between measured and predicted flow velocity as well as hematocrit (normalized relative velocity deviation, 1.57±0.14; normalized hematocrit deviation, 1.06±0.05; mean±SEM; not shown in Fig 4).

Fig 4 also gives the results for model simulations assuming a constant viscosity in all vessel segments, independent of diameter, hematocrit, or shear rate. This viscosity law, which does not exhibit any decrease in viscosity with decreasing diameter (Fahraeus-Lindqvist effect), leads to a slight reduction of deviation

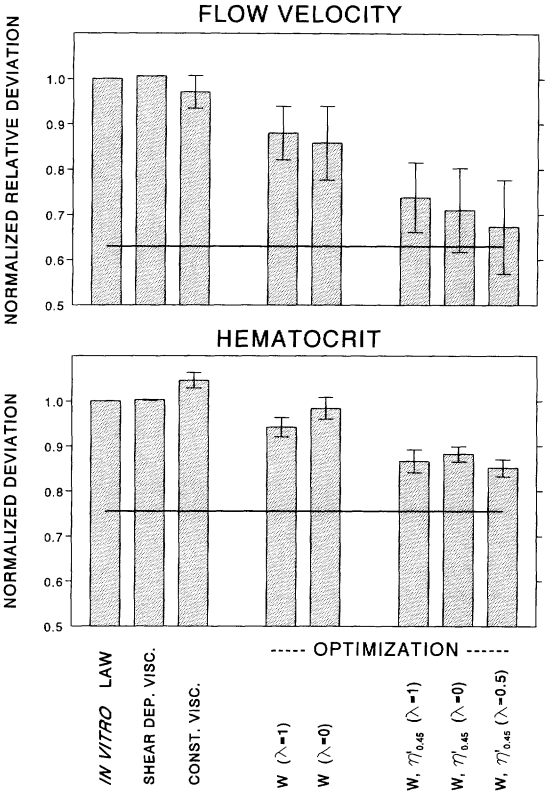

FIG 4. Bar graphs showing minimization of systematic deviations (mean±SEM) between measured and predicted flow velocity (top, n=3 networks) and discharge hematocrit (bottom, n=6 networks) by modification of the viscosity law used in the mathematical flow simulations. The continuous horizontal line indicates the level of the combined stochastic error; the additional deviation above that line, the systematic deviation, is attributed to inadequacies of the rheological laws used in the simulation, especially the viscosity law. From left to right, data are given for (1) calculations based on the in vitro viscosity law, (2) a viscosity law with added shear dependence of viscosity (shear dep. visc.), (3) a viscosity law assuming identical viscosity in all segments irrespective of diameter, hematocrit, or shear rate (const. visc.), and (4) a number of viscosity laws based on optimized values for the parameters W (bars 4 through 8) and $\eta'_{0.45}$ (bars 6 through 8). W is used to modify the diameter dependence of viscosity and has the dimension of a length, λ is a parameter determining the hematocrit dependence of viscosity, and $\eta'_{0.45}$ is viscosity for a fixed discharge hematocrit of 0.45 (see text).

in flow velocity and a slight increase of the hematocrit deviation compared with the in vitro viscosity law.

Modified Viscosity Law

In the next step, the viscosity law as given in Equation 3 was modified by adding a diameter-dependent term to the original parametric description of the in vitro data:

$$(8)\qquad \eta_{mod}=\left[1+(\eta_{0.45}-1)\cdot\frac{(1-H_D)^C-1}{(1-0.45)^C-1}\cdot\left(\frac{D}{D-W}\right)^{4\lambda}\right]\cdot\left(\frac{D}{D-W}\right)^{4(1-\lambda)}$$

where η_{mod} is modified viscosity, W has the dimension of a length, and λ is a constant. Our rationale for modifying Equation 3 in this way can be explained by considering its properties for different values of λ. At $\lambda=0$, the first W-dependent term equals unity, and W can be interpreted as a reduction of the hydrodynamically effective vessel diameter leading to a reduction of vessel conductance independent of hematocrit. This could, for instance, be effected by macromolecular structures bound to the endothelial surface retarding or impeding flow close to the vessel wall. The optimal value of W was determined by minimizing the deviation of flow velocity for the networks in which velocities were measured (n=3), leading to an average value of 0.67±0.33 μm (mean±SD). For the remaining three networks, the deviation of hematocrit was minimized. The average value of W from all six networks was 0.84±0.26 μm. The corresponding deviations of both flow velocity and hematocrit (Fig 4) were reduced compared with those obtained for the in vitro viscosity law.

It cannot, however, be assumed that the discrepancy between the in vitro viscosity law and the effective viscosity in vivo is exclusively the result of a reduction of hydrodynamically effective vessel diameter relative to the measured diameter. On the contrary, it is likely that red blood cells and their deformation and interaction with each other as well as with the vessel wall and its surface structures during perfusion play a major role in establishing in vivo viscosity relations. Such interactions can be accounted for in Equation 8 by setting λ to values above zero, rendering the impact of W on viscosity hematocrit dependent. The extreme case in which a hypothetical discrepancy between in vivo and in vitro viscosity completely relies on the presence and concentration of blood cells corresponds to $\lambda=1$. Optimization of W for $\lambda=1$ led to velocity and hematocrit deviations similar to those obtained for $\lambda=0$ (Fig 4).

Irrespective of the λ value used, the viscosity (η_{mod}) calculated from Equation 8 by using the optimized values of W increases with decreasing vessel diameter in a range far above the range where minimum viscosities are seen in vitro (6 to 7 μm). Therefore, a viscosity law that did not incorporate an intrinsic reduction of viscosity with decreasing vessel diameter according to the Fahraeus-Lindqvist effect was tested. This was achieved by replacing, in Equation 8, the diameter-dependent $\eta_{0.45}$ from Equation 4 with a constant value, $\eta'_{0.45}$. A two-dimensional optimization procedure (downhill simplex method) was then used to find the values of $\eta'_{0.45}$ and W that minimized the systematic deviation between measured and predicted velocities if available (three networks) or hematocrit. Optimizations were performed for λ, increasing in steps of 0.25 from 0 to 1.

As Fig 4 shows, this change resulted in a substantial additional decrease in deviations, whether λ was set to 0, 0.5, or 1. Minimal deviations for both flow velocity and hematocrit were obtained at $\lambda=0.5$ (velocity: relative rms deviation, 0.60±0.02 [mean±SEM]; hematocrit: absolute rms deviation, 0.16±0.09). The corresponding optimal parameter values were W=1.09±0.57 μm and $\eta'_{0.45}$=1.98±0.16 (mean±SD; n=3; values are given for the networks in which velocities were measured). This indicates that both red blood cell–dependent and –independent phenomena contribute to the discrepancy between in vitro and in vivo effective viscosity. By use of the modified viscosity law described by Equation 8 and the optimal values for λ, W, and $\eta'_{0.45}$, the respective velocity deviations nearly reach the minimum level indicated by the combined measurement error and model input error. This demonstrates that the systematic deviation due to inadequacies of the rheological laws used in the simulation process could be nearly eliminated by appropriate changes of the viscosity law.

The modified viscosity law derived in the above-described optimization uses the dependence of viscosity on hematocrit as defined by parameter C given in Equation 5 for the in vitro viscosity law. To test the impact of this relation on the deviation between measured and predicted flow velocity and hematocrit, optimizations of W and $\eta'_{0.45}$ for $\lambda=0.5$ were performed by using several constant C values between −0.8 and +1. The lowest deviations obtained with constant values of C were obtained for C=0.1, however, still being slightly higher than those obtained with the in vitro relation between C and vessel diameter.

The modified viscosity law based on the average values obtained by the optimization process for W, $\eta'_{0.45}$, and λ is compared with the in vitro viscosity law in Fig 5. Significant information on effective viscosity is obtained from the in vivo optimization only in a diameter range covered by sufficient numbers of vessel segments in the microvessel networks used for the analysis. This range starts at ≈4 μm and extends to ≈25 μm for arterioles and to ≈40 μm for venules. The two viscosity laws exhibit substantial differences in this diameter range. Much higher effective viscosities are predicted by the in vivo optimization compared with the in vitro viscosity law, especially for vessel diameters ranging from 4 to 10 μm, where the in vitro viscosity shows its minimum. In addition, a strong hematocrit dependence is seen in the modified viscosity law.

Shear-Rate Dependence

As stated earlier, the addition of a shear-rate–dependent component to the in vitro viscosity law according to data obtained in vivo[28] led to substantial increases of the deviation between measured and predicted results. The impact of shear-rate–dependent viscosity laws was tested in more detail by optimizing the parameters P and Q of Equation 7 for the three network databases containing measured velocity data. The optimization was started from the viscosity law given by Equation 8 using the optimal values for the parameters W, $\eta'_{0.45}$, and λ described above. Minimal systematic deviations between measured and predicted velocities were ob-

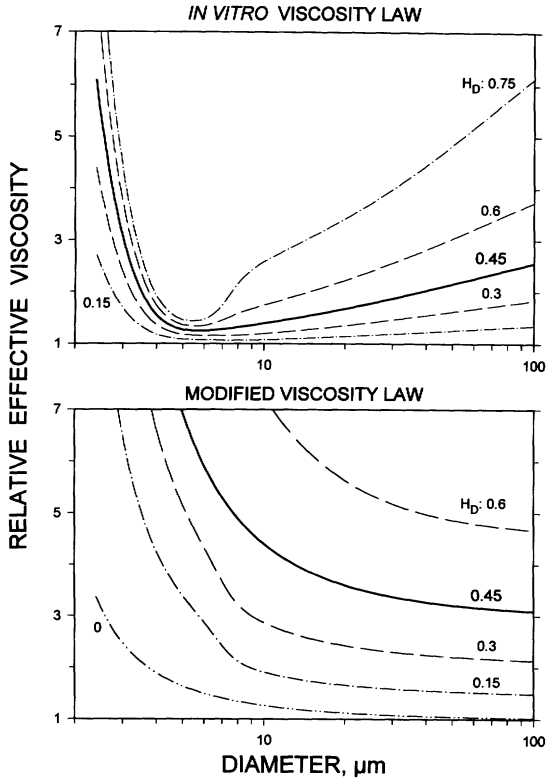

FIG 5. Graphs showing relative effective viscosity as a function of diameter and hematocrit as given by the in vitro viscosity law (top) and the modified viscosity law using the optimized values for λ, W, and $\eta'_{0.45}$ (λ=0.5, W=1.09 μm, and $\eta'_{0.45}$=1.98; W is used to modify the diameter dependence of viscosity and has the dimension of a length, λ is a parameter determining the hematocrit dependence of viscosity, and $\eta'_{0.45}$ is viscosity for a fixed discharge hematocrit [H_D] of 0.45 (bottom). The corresponding equations in the text (Equations 5 and 8) give a viscosity/diameter relation valid for human red blood cells (mean corpuscular volume [MCV], ≈92 fL). To adapt the results for the smaller rat red blood cells (MCV, ≈55 fL), the diameter values used in the respective equations during simulation and shown on this figure have been scaled down according to the ratio of the cube root of the respective MCV values [$(55/92)^{1/3}$≈0.84]. The modified law exhibits a strong viscosity increase with decreasing diameter. In addition, the viscosity values are much higher than those given by the in vitro viscosity law, especially for vessel diameters below ≈20 μm.

tained at mean±SEM values for P (0.17±0.06) and Q (−0.87±0.02). At these values, the shear-rate dependence of viscosity is even weaker than that in the original data of Reinke et al.[26] Although very low shear rates (0.1 s^{-1}) are found in some vessels of the networks analyzed, the mean shear-rate levels are ≈3 orders of magnitude higher (arterioles, 147±135 s^{-1}; capillaries, 103±166 s^{-1}; venules, 62±60 s^{-1}; mean±SD). These results suggest that shear-dependent components of viscosity play only a very limited role under the perfusion conditions present here.

In Vivo Viscosity Law

The modified viscosity law shown in Fig 5 loses significance for vessel diameters above ≈30 μm. On the other hand, the mechanisms underlying the observed high resistance in vivo will probably be related to interactions between the flowing blood and the vessel walls and therefore become less relevant with increasing vessel diameter. It is also consistent with the data from

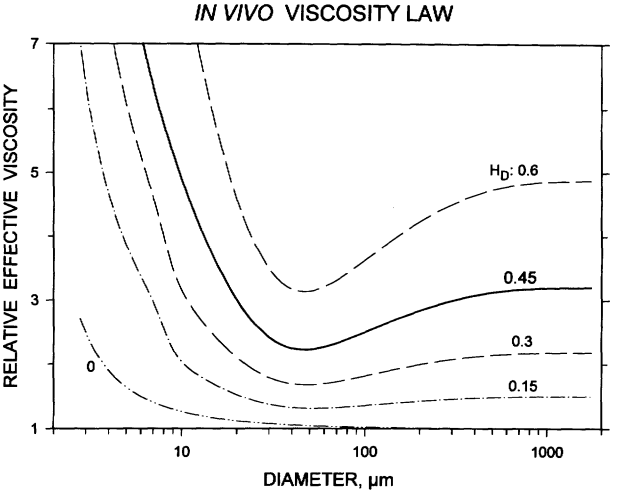

FIG 6. Graph showing relative effective blood viscosity as described by the in vivo viscosity law (Equations 5, 9, and 10). The viscosity values shown for a given diameter directly apply to blood with a mean corpuscular volume of ≈92 fL, typical for human blood.

direct measurements of viscosity in microvessel segments[15,16] to assume that in a diameter range above ≈50 μm, the in vitro viscosity law adequately describes the resistance to blood flow in vivo. Therefore, a combined law describing the effective resistance to blood flow in vivo as a function of vessel diameter and hematocrit was derived by using the modified viscosity law, which was optimized to match the in vivo rheology of blood for diameters below ≈20 μm and the in vitro viscosity law for diameters above ≈50 μm. In the intermediate diameter range, a smooth transition between both viscosity laws was attempted. This was achieved by using constant values for λ and W according to those obtained in the optimization (λ=0.5, W=1.1 μm) and changing two parameters in the in vitro description of the Fahraeus-Lindqvist effect (Equation 4) appropriately.

The resulting combined in vivo viscosity law is given as

$$\eta_{vivo}=\left[1+(\eta^*_{0.45}-1)\cdot\frac{(1-H_D)^C-1}{(1-0.45)^C-1}\cdot\left(\frac{D}{D-1.1}\right)^2\right]\cdot\left(\frac{D}{D-1.1}\right)^2 \quad (9)$$

where η_{vivo} is in vivo viscosity and with $\eta^*_{0.45}$ defined as follows:

$$\eta^*_{0.45}=6\cdot e^{-0.085D}+3.2-2.44\cdot e^{-0.06D^{0.645}} \quad (10)$$

The in vivo viscosity law is illustrated in Fig 6. Effective viscosity decreases with decreasing vessel diameter according to the Fahraeus-Lindqvist effect only down to diameters of ≈20 to 30 μm. The minimal effective viscosities reached in vivo are much higher than those obtained from the in vitro viscosity law. Simulation runs using the combined in vivo viscosity law led to deviations of velocity and hematocrit that were even slightly lower than those obtained with the modified viscosity law shown in the lower panel of Fig 5.

Experimental Measurements of Network Resistance and Pressure Drop

The results of direct resistance measurements, obtained in a separate series of experiments, are shown in

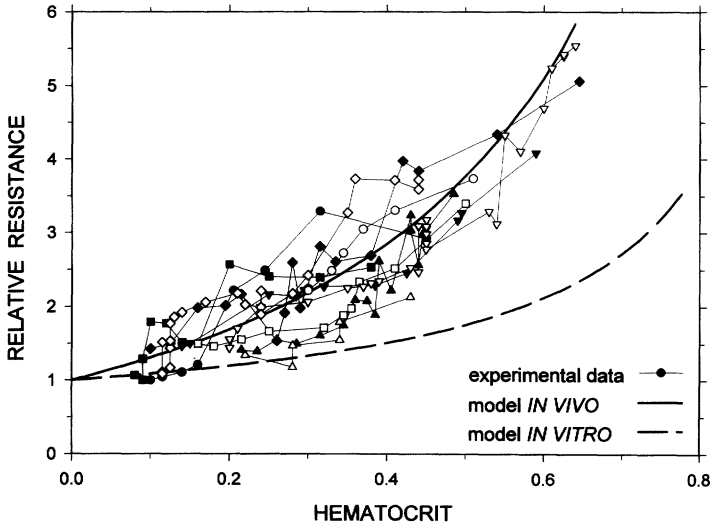

FIG 7. Graph showing flow resistance across microvascular networks as a function of systemic hematocrit. Given are results from experimental determinations of pressure drop and volume flow in 10 microvascular networks (experimental data, different symbol for each network) together with predictions of the model simulation for the 6 microvessel networks analyzed for morphology and topology of all vessel segments on the basis of in vivo and in vitro viscosity laws, respectively.

Fig 7. In 10 microvascular networks, arteriolar and venular pressures and the arteriolar volume flow rate were determined at artificially modified levels of H_S. The microvascular networks used in this set of experiments were similar to those of the network analysis, with regard to the diameter of the feeding arteriole (resistance experiments, 29±5 μm [mean±SD], network analysis, 30±3 μm), the draining venule (resistance experiments, 55±13 μm; network analysis, 49±13 μm), and the total volume flow rate perfused through the network (resistance experiments, 843±607 nL/min; network analysis, 774±379 nL/min). The systemic blood pressure before the start of the hemoconcentration and dilution procedures averaged 134±11 mm Hg. Hemoconcentration was performed in 7 networks and led to an increase in systemic pressure by 11±6 mm Hg. The minimal systemic pressures reached at the end of the dilution procedure averaged 84±18 mm Hg. These changes of systemic blood pressure were accompanied by comparatively small decreases in volume flow rate through the networks, which averaged 3.8±12.5% from the highest to the lowest hematocrit level, indicating nearly constant levels of shear rate throughout the experiments.

The data from each network were normalized with respect to the resistance value extrapolated to $H_S=0$ for that network. The number of individual resistance measurements per experiment ranged from 7 to 30 (total number, 138), and the systemic hematocrit varied between 0.15±0.06 and 0.49±0.08 (minimal H_S, 0.08; maximal H_S, 0.68). To allow a comparison with the simulation results, predictions of flow resistance obtained by the mathematical model simulation using the in vivo and the in vitro viscosity laws are given in Fig 7 as average values for the six microvascular networks for which complete databases were available. Both the direct experimental data and the model simulations based on the in vivo viscosity law show a marked dependence of network flow resistance on H_S. This agreement indicates that the high flow resistance determined experimentally and calculated from the in vivo viscosity law is not primarily created by a systematic underestimation of vessel diameters or by a cell-independent rheological phenomenon.

Fig 8 compares the values of the directly measured pressure drop across microvascular networks in the rat mesentery with predictions by the model simulation. Under control conditions, the mean arteriolar input and venular draining pressures determined by micropuncture were 75.7±17.5 and 13.8±3.3 mm Hg, respectively, corresponding to a pressure drop of 61.9±16.7 mm Hg (mean±SD). Extrapolation to $H_S=0$ using a fit to the experimental data according to Equation 6 yielded a pressure drop of 21.3 mm Hg. The corresponding predictions of the model simulation are given for the three networks in which flow velocities were measured. By use of the in vitro viscosity law, a pressure drop of 23.8±6 mm Hg was obtained for $H_S=0.39\pm0.06$; the in vivo

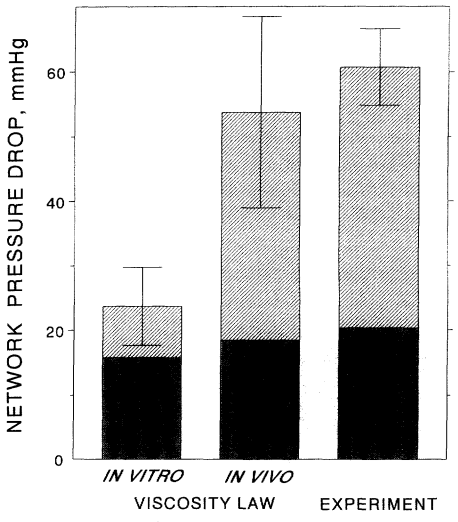

FIG 8. Bar graph showing pressure difference (mean±SEM) between feeding arterioles and draining venules calculated for three networks of the rat mesentery with the flow simulation model using the in vitro viscosity law (left bar) and the in vivo viscosity law (middle bar). The dark portion of each bar represents the pressure drop calculated for flow of pure plasma; the hatched part corresponds to the additive cell-dependent flow resistance at an input hematocrit of ≈0.39. The right bar shows the mean pressure drop determined by micropressure measurement. Here, the pressure drop for pure plasma flow was extrapolated by using a fit to the experimental data according to Equation 6.

viscosity law yielded 53.7±14.8 mm Hg. The corresponding values for H_S=0 were as follows: in vitro viscosity law, 15.9±3.8 mm Hg; in vivo viscosity law, 18.4±4.5 mm Hg.

The values for pure plasma flow (H_S=0) show good agreement between experimental data and both model simulations. For normal levels of systemic hematocrit, however, only the simulation based on the in vivo viscosity law agrees with the results of direct pressure measurements. The somewhat higher pressure drop found by micropressure measurements could be related to the higher H_S in these experiments (H_S=0.42±0.02 [mean±SD] compared with 0.39±0.06 in the experiments used for the network analysis).

Discussion

Viscosity and Flow Resistance

The present results demonstrate that the flow resistance in microvessels in vivo is much higher than predicted from rheology of blood in glass tubes. The ratio of viscosities in individual microvessels perfused with blood at a hematocrit of 0.4 relative to that obtained in equally sized glass tubes ranges between ≈2 at a diameter of 20 μm and 8 at diameters of ≈5 μm (Figs 5 and 6). According to model simulations, the average pressure drop across microvascular networks (flow-weighted pressure difference between feeding arteriolar and draining venular vessel segments) is more than doubled when the new in vivo viscosity law is used instead of the in vitro law (Fig 8). Most of this difference is related to the flow resistance generated in the presence of blood cells. Estimates of pressure drop obtained from the model using the in vivo viscosity law are fairly close to the values obtained here by direct measurements of pressure drop and volume flow for mesenteric microvascular networks and to values derived from microvascular pressure profiles for the cat mesentery[29] for similar-sized arterioles and venules. These results strongly suggest that the flow resistance of small microvessels in vivo is indeed much higher than predictions derived solely on the basis of rheological measurements in long straight glass tubes in vitro.

Because of experimental difficulties, only a few attempts have been made to directly measure the effective blood viscosity in vivo. Lipowsky and colleagues[14,15] assessed in vivo blood viscosity in single unbranched microvessels by combining a double micropipette differential pressure measurement with determination of v_{cl} using an optical dual-window method. They report data for microvessels ranging in diameter from ≈60 μm down to 7 μm. The individual data points, however, show a very high scatter and do therefore not allow detailed analyses of diameter- and hematocrit-dependent changes of viscosity. The average viscosity value given for 55 microvessel segments (diameter, 29.8±14.2 μm) is 4.22±2.35 cp. When the reported plasma viscosity of ≈1 cp is taken into account, these values directly translate into relative effective blood viscosities that are even higher than those predicted by the present in vivo viscosity law for a hematocrit of 0.45. This indicates that the in vivo viscosity law presented here, which predicts much higher viscosities for vessels <30 μm than reported from tube flow studies, does not overestimate actual flow resistance in living microvessels.

Factors Influencing Effective Viscosity

The apparent viscosity of blood in narrow glass tubes is not an intrinsic property of the blood but reflects the combined property of the system, ie, the tube of a given geometry and the blood consisting of cells suspended in plasma. Similarly, the effective viscosity of blood in a microvessel, as defined in the present study, is a measure of the flow resistance resulting from physical processes occurring during blood flow through a vessel in the microcirculatory network. Estimates of effective viscosity, therefore, contain no direct information on the mechanisms involved or on the reasons for the observed discrepancies between effective viscosity in vivo and apparent viscosity in vitro. Although these mechanisms are not yet known, it is possible to list a number of factors that may contribute:

(1) Macromolecules on the inner endothelial surface (endo-endothelial layer[30,31]) may impede flow in near-wall regions of microvessels, either by increasing the local viscosity or by temporarily sticking to passing blood cells.

Substantial increases of H_T in muscle capillaries have been seen during experimental procedures leading to a large increase in volume flow rate, such as vasodilation with adenosine[32] or muscle exercise.[33] Desjardins and Duling[32] reported similar hematocrit increases after perfusion of the microvessels with heparinase and therefore speculated that a macromolecular layer on the endothelial surface reducing the effective vessel radius, which might be fairly thick in resting flow states, changes its molecular organization, leading to a lower width during high flow states. Although in our experiments there is no indication that such a layer might reduce the cross-sectional area of microvessels accessible to the flow of red blood cells, such a layer might nevertheless impede flow to varying degrees, dependent on overall flow velocity. Siegel et al[34] showed that proteoglycans on the endothelial surface may indeed change their spatial organization with changes of shear stress. The possibility of interactions between the endothelial surface and components of the flowing blood or plasma is shown by Reinhart et al.[35] They reported a decrease in the sinking velocity of suspended microbeads covered with endothelial cells in the presence of plasma in the suspending medium.

(2) The inner vessel contour is irregular. Therefore, the hydrodynamically effective vessel diameter is smaller than the experimentally measured average vessel diameter.[36,37] The irregularity of the inner vessel contour will also lead to a rearrangement of red blood cells in the blood flowing through the vessel, which might cause additional energy dissipation.

In this context, it is noteworthy that the present results were obtained in maximally vasodilated microvessel networks. Since irregularities of vessel diameters will be enhanced by increased activity of vascular smooth muscle, the discrepancies between resistance to flow in vitro and in vivo might even be more obvious if beds exhibiting higher vascular tone are considered.

(3) The average length of vessel segments in the rat mesentery is of the order of 350 μm compared with a tube length of several millimeters or even centimeters in most in vitro studies. Each branch point leads to a perturbation of the velocity and concentration profiles

in the downstream vessels. It can be assumed that each asymmetry of hematocrit or velocity profiles leads to additional energy dissipation compared with the fully developed flow in long, straight glass tubes.[38-40]

(4) White cells, which are removed from blood samples used in most tube flow studies in vitro, might have an impact on the effective flow resistance in vivo. For skeletal muscle, model studies and experimental observations have suggested an increase of resistance that is due to the presence of white cells ranging from ≈1% to 20%.[27,41-45] However, in the mesenteric microcirculation, the impact of white cells on flow resistance is probably much more limited because of the comparatively large size of mesenteric capillaries.[46] In the microvascular networks analyzed here, a mean±SD capillary diameter 8.7±2.4 μm was found compared with a value of 5.4±1 μm reported by Warnke and Skalak[41] for the rat spinotrapezius muscle.

Implications of the In Vivo Viscosity Law

In vitro measurements of apparent blood viscosity have often been used as a basis for interpreting aspects of circulatory function. Our finding of substantially different behavior in vivo is therefore likely to lead to new interpretations in some areas, including the following three examples.

The in vitro and in vivo viscosity laws show a large difference in the relation between diameter and effective viscosity (Fahraeus-Lindqvist effect). Although viscosity decreases with tube diameter down to 7 μm in vitro, minimal viscosities in vivo are reached at vessel diameters of ≈30 μm. This finding has implications that are relevant to the regulation of peripheral perfusion: Arterioles with vessel diameters below ≈30 μm represent the major site for the control of peripheral resistance. If such vessels constrict, eg, from 20 to 10 μm, the in vivo viscosity law predicts an increase of effective viscosity rather than a decrease as expected from in vitro measurements. The resulting increase of flow resistance, which results from both the elevated geometric hindrance and the changes of effective blood viscosity, is approximately twice that predicted by the in vitro viscosity law. Therefore, the present findings place a much higher emphasis than hitherto accepted on the importance of blood viscosity as a determinant of peripheral perfusion and a component of blood flow regulation.

As shown in Fig 8, the in vitro and in vivo viscosity laws exhibit very similar pressure drops across microvascular networks for pure plasma flow (H_S=0). However, differences between predictions of the two laws are prominent at normal systemic hematocrits, implying that the higher resistance in microvessels in vivo is mainly dependent on the presence of red blood cells. A further implication is that resistance to flow in microvascular beds is much more sensitive to hematocrit than would be expected on the basis of data obtained when using narrow glass tubes. Our findings provide a basis for reassessing the consequences of systemic hemodilution for perfusion of peripheral beds.

If macromolecules on the endothelial surface contribute to in vivo flow resistance (possible mechanism 1, above), then flow resistance in microvascular beds may be modulated through modifications of the endo-endothelial layer, even in the absence of diameter changes. The existence of such a mechanism would have important implications both for the understanding of flow regulation in normal and pathological conditions and for the potential development of methods to improve tissue perfusion.

Acknowledgments

This study was supported by Deutsche Forschungsgemeinschaft (Pr 271/1-1, 1-2 and 5-1) and by National Institutes of Health grant HL-34555. The technical help of B. Giesicke and the assistance of A. Scheuermann in preparing the manuscript are gratefully acknowledged.

References

1. Poiseuille JLM. *Recherches sur la Force du Cœur Aortique.* Paris, France: Didot le Jeune; 1828. Dissertation.
2. Poiseuille JLM. Recherches sur les causes du mouvement du sang dans les veines. *J Physiol Exp Pathol.* 1830;10:277-295.
3. Brooks DE, Goodwin JW, Seaman GVF. Interactions among erythrocytes under shear. *J Appl Physiol.* 1970;28:172-177.
4. Chien S, Usami S, Dellenback RJ, Bryant CA. Comparative hemorheology: hematological implications of species differences in blood viscosity. *Biorheology.* 1971;8:35-57.
5. Chien S. Biophysical behaviour of red cells in suspensions. In: Surgenor DMN, ed. *The Red Blood Cell, II.* New York, NY: Academic Press Inc; 1975:1031-1133.
6. Martini P, Pierach A, Schreyer E. Die Strömung des Blutes in engen Gefäßen: Eine Abweichung vom Poiseuille'schen Gesetz. *Dtsch Arch Klin Med.* 1930;169:212-222.
7. Fahraeus R, Lindqvist T. The viscosity of the blood in narrow capillary tubes. *Am J Physiol.* 1931;96:562-568.
8. Bayliss LE. Rheology of blood and lymph. In: Frey-Wissling A, ed. *Deformation and Flow in Biological Systems.* Amsterdam, Netherlands: North-Holland; 1952:355-418.
9. Prothero JW, Burton AC. The physics of blood flow in capillaries, II: the capillary resistance to flow. *Biophys J.* 1962;2:199-212.
10. Gerbstädt H, Vogtmann C, Rüth P, Schöntube E. Die Scheinviskosität von Blut in Glaskapillaren kleinster Durchmesser. *Naturwissenschaften.* 1966;53:526.
11. Braasch D, Jenett W. Erythrozytenflexibilität, Hämokonzentration und Reibungswiderstand in Glaskapillaren mit Durchmessern zwischen 6 bis 50 μm. *Pflugers Arch.* 1968;302:245-254.
12. Cokelet GR. Macroscopic rheology and tube flow of human blood. In: Grayson J, Zingg W, eds. *Microcirculation.* New York, NY: Plenum Publishing Corp; 1976;1:9-31.
13. Pries AR, Neuhaus D, Gaehtgens P. Blood viscosity in tube flow: dependence on diameter and hematocrit. *Am J Physiol.* 1992;263: H1770-H1778.
14. Lipowsky HH, Zweifach BW. Methods for the simultaneous measurement of pressure differentials and flows in single unbranched microvessels for rheological studies. *Microvasc Res.* 1977;14: 345-361.
15. Lipowsky HH, Kovalcheck S, Zweifach BW. The distribution of blood rheological parameters in the microcirculation of cat mesentery. *Circ Res.* 1978;43:738-749.
16. Lipowsky HH, Usami S, Chien S. In vivo measurements of 'apparent viscosity' and microvessel hematocrit in the mesentery of the cat. *Microvasc Res.* 1980;19:297-319.
17. Pries AR, Ley K, Gaehtgens P. Generalization of the Fahraeus principle for microvessel networks. *Am J Physiol.* 1986;251:H1324-H1332.
18. Ley K, Pries AR, Gaehtgens P. A versatile intravital microscope design. *Int J Microcirc Clin Exp.* 1987;6:161-167.
19. Pries AR, Kanzow G, Gaehtgens P. Microphotometric determination of hematocrit in small vessels. *Am J Physiol.* 1983;245: H167-H177.
20. Pries AR. A versatile video image analysis system for microcirculatory research. *Int J Microcirc Clin Exp.* 1988;7:327-345.
21. Pries AR, Eriksson SE, Jepsen H. Real-time oriented image analysis in microcirculatory research. *SPIE.* 1990;1357:257-263.
22. Goodman AH, Guyton AC, Drake R, Loflin JH. A television method for measuring capillary red cell velocities. *J Appl Physiol.* 1974;37:126-130.
23. Pries AR, Secomb TW, Gaehtgens P, Gross JF. Blood flow in microvascular networks: experiments and simulation. *Circ Res.* 1990;67:826-834.

24. Pittman RN, Ellsworth ML. Estimation of red cell flow in microvessels: consequences of the Baker-Wayland spatial averaging model. *Microvasc Res.* 1986;32:371-388.
25. Pries AR, Ley K, Claaßen M, Gaehtgens P. Red cell distribution at microvascular bifurcations. *Microvasc Res.* 1989;38:81-101.
26. Reinke W, Gaehtgens P, Johnson PC. Blood viscosity in small tubes: effect of shear rate, aggregation, and sedimentation. *Am J Physiol.* 1987;253:H540-H547.
27. Warnke KC, Skalak TC. The effects of leukocytes on blood flow in a model skeletal muscle capillary network. *Microvasc Res.* 1990;40: 118-136.
28. Lipowsky HH. Network hemodynamics and the shear rate dependency of blood viscosity. In: Popel AS, Johnson PC, eds. *Microvascular Networks: Experimental and Theoretical Studies.* Basel, Switzerland: S Karger AG; 1986;182-196.
29. Zweifach BW, Lipowsky HH. Quantitative studies of microcirculatory structure and function, III: microvascular hemodynamics of cat mesentery and rabbit omentum. *Circ Res.* 1977;41:380-390.
30. Copley AL. Hemorheological aspects of the endothelium-plasma interface. *Microvasc Res.* 1974;8:192-212.
31. Copley AL, Staple PH. Hemorheological studies on the plasmatic zone in the microcirculation of the cheek pouch of Chinese and Syrian hamsters. *Biorheology.* 1962;1:3-14.
32. Desjardins C, Duling BR. Heparinase treatment suggests a role for the endothelial cell glycocalyx in regulation of capillary hematocrit. *Am J Physiol.* 1990;258:H647-H654.
33. Klitzman B, Duling BR. Microvascular hematocrit and red cell flow in resting and contracting striated muscle. *Am J Physiol.* 1979; 237:H481-H490.
34. Siegel G, Walter A, Rückborn K, Buddecke E, Schmidt A, Gustavsson H, Lindman B. NMR studies of cation induced conformational changes in anionic biopolymers at the endothelium-blood interface. *Polymer J.* 1991;23:697-708.
35. Reinhart WH, Boulanger CM, Lüscher TF, Haeberli A, Straub PW. Influence of endothelial surface on flow velocity in vitro. *Am J Physiol.* 1993;265:H523-H529.
36. Cokelet GR, Sarelius IH. Perceived vessel lumen and cell-blood velocity ratio: impact on in vivo blood flow rate determination. *Am J Physiol.* 1992;262:H1156-H1163.
37. Kiani MF, Cokelet GR, Sarelius IH. Effect of diameter variability along a microvessel segment on pressure drop. *Microvasc Res.* 1993;45:219-232.
38. Zweifach BW. Quantitative studies of microcirculatory structure and function, I: analysis of pressure distribution in the terminal vascular bed in cat mesentery. *Circ Res.* 1974;34:843-857.
39. Zweifach BW. Quantitative studies of microcirculatory structure and function, II: direct measurement of capillary pressure in splanchnic mesenteric vessels. *Circ Res.* 1974;34:858-866.
40. Kiani MF, Cokelet GR. Additional pressure drop at a bifurcation due to the passage of flexible disks in a large scale model. *J Biomech Eng.* 1994. In press.
41. Warnke KC, Skalak TC. Leukocyte plugging in vivo in skeletal muscle arteriolar trees. *Am J Physiol.* 1992;262:H1149-H1155.
42. Braide M, Amundson B, Chien S, Bagge U. Quantitative studies on the influence of leukocytes on the vascular resistance in a skeletal muscle preparation. *Microvasc Res.* 1984;27:331-352.
43. Braide M, Blixt Å, Bagge U. Leukocyte effects on the vascular resistance and glomerular filtration of the isolated rat kidney at normal and low flow states. *Circ Shock.* 1986;20:71-80.
44. Fenton BM, Wilson DW, Cokelet GR. Analysis of the effects of measured white blood cell entrance times on hemodynamics in a computer model of a microvascular bed. *Pflugers Arch.* 1985;403: 396-401.
45. Sutton DW, Schmid-Schönbein GW. In skeletal muscle microcirculation the additional pressure drop per granulocyte is about 1000 times that of an erythrocyte. *FASEB J.* 1990;4:A287. Abstract.
46. Gaehtgens P, Pries AR. Leukocyte flow and capillary perfusion in microvascular networks. *Prog Appl Microcirc.* 1991;18:46-58.

Resistance to blood flow in microvessels in vivo.

A R Pries, T W Secomb, T Gessner, M B Sperandio, J F Gross and P Gaehtgens

Circ Res. 1994;75:904-915
doi: 10.1161/01.RES.75.5.904
Circulation Research is published by the American Heart Association, 7272 Greenville Avenue, Dallas, TX 75231

Print ISSN: 0009-7330. Online ISSN: 1524-4571